

# Charged-current weak interaction processes in hot and dense matter and its impact on the spectra of neutrinos emitted from proto-neutron star cooling

G. Martínez-Pinedo,<sup>1,2</sup> T. Fischer,<sup>2,1</sup> A. Lohs,<sup>1</sup> and L. Huther<sup>1</sup>

<sup>1</sup>*Institut für Kernphysik, Technische Universität Darmstadt,  
Schlossgartenstraße 2, 64289 Darmstadt, Germany*

<sup>2</sup>*GSI Helmholtzzentrum für Schwerionenforschung, Planckstraße 1, 64291 Darmstadt, Germany*  
(Dated: March 3, 2013)

We have performed three-flavor Boltzmann neutrino transport radiation hydrodynamics simulations covering a period of 3 s after the formation of a protoneutron star in a core-collapse supernova explosion. Our results show that a treatment of charged-current neutrino interactions in hot and dense matter as suggested by Reddy *et al.* [Phys. Rev. D **58**, 013009 (1998)] has a strong impact on the luminosities and spectra of the emitted neutrinos. When compared with simulations that neglect mean field effects on the neutrino opacities, we find that the luminosities of all neutrino flavors are reduced while the spectral differences between electron neutrino and antineutrino are increased. Their magnitude depends on the equation of state and in particular on the symmetry energy at sub-nuclear densities. These modifications reduce the proton-to-nucleon ratio of the outflow, increasing slightly their entropy. They are expected to have a substantial impact on the nucleosynthesis in neutrino-driven winds, even though they do not result in conditions that favor an *r*-process. Contrarily to previous findings, our simulations show that the spectra of electron neutrinos remain substantially different from those of other (anti)neutrino flavors during the entire deleptonization phase of the protoneutron star. The obtained luminosity and spectral changes are also expected to have important consequences for neutrino flavor oscillations and neutrino detection on Earth.

PACS numbers: 26.30.Jk, 97.60.Bw, 26.50.+x, 26.30.-k

Supernova explosions of massive stars are related to the birth of neutron stars due to the collapse of the stellar core at the end of stellar evolution [2]. The detection of neutrinos from SN1987A [3] confirmed that the  $\approx 3 \times 10^{53}$  ergs of gravitational energy gained by the core collapse are emitted as neutrino radiation on time scales of tens of seconds, during which the central protoneutron star (PNS) cools, deleptonizes and contracts. In the delayed neutrino-heating explosion mechanism [2, 4], neutrinos also transport energy from the nascent PNS to the stalled bounce shock. This mechanism remains the most viable scenario to explain supernova explosions as confirmed by recent two-dimensional simulations [5]. Once the explosion sets in, the continuous emission of neutrinos from the PNS drives a low-mass outflow known as neutrino-driven wind [6] that is currently considered the favored site for the productions of elements heavier than iron (e.g. [7]). As neutrinos travel through the stellar mantle, they can suffer flavor oscillations [8], contribute to the nucleosynthesis of several rare isotopes [9] and even drive an *r* process in the He-shell of metal-poor stars [10] before they are finally detected on Earth.

Accounting for all aspects discussed above requires the knowledge of the spectra of the neutrinos emitted during the cooling phase of the PNS. Due to their low energies  $\nu_{\mu,\tau}, \bar{\nu}_{\mu,\tau}$  interact only via neutral-current reactions. Hence, together with the neutron-richness of the PNS surface one expects the following neutrino-energy hierarchy:  $\langle E_{\nu_{\mu,\tau}} \rangle > \langle E_{\bar{\nu}_e} \rangle > \langle E_{\nu_e} \rangle$  [11, 12], with  $\langle E \rangle$  the average energy of the neutrino spectrum. Early supernova models [13] predicted large energy differences be-

tween  $\bar{\nu}_e$  and  $\nu_e$  that resulted in neutron-rich ejecta as required by *r*-process nucleosynthesis [14]. However, as the treatment of neutrino transport and weak interaction processes improved, the computed energy difference between  $\bar{\nu}_e$  and  $\nu_e$  decreased and the early wind ejecta became proton rich [15]. More recently, it has been possible to perform supernova simulations based on three-flavor Boltzmann neutrino transport for time scales of several tens of seconds [16, 17], covering the whole deleptonization of the PNS. These simulations predict a continuous decrease of the energy difference between neutrinos and antineutrinos of all flavors that became practically indistinguishable after  $\approx 10$  s. The exact value depends on the progenitor. The proton-richness of the ejecta increases continuously with time and leaves the  $\nu p$  process [18] as the only mechanism for producing elements heavier than iron in neutrino-driven winds.

The simulations of ref. [17] have been recently analyzed, showing that the convergence of neutrino and antineutrino spectra at late times is due to the suppression of charged-current processes at high densities [12]. This analysis was based on a set of neutrino opacities that assume a non-interacting gas of nucleons and nuclei. This approximation may be valid during the accretion phase prior to the onset of the supernova explosion when the region from where neutrinos decouple, the neutrinospheres, is located at relatively low densities,  $\sim 10^{11}$  g cm<sup>-3</sup>. However, as the PNS cools the neutrinospheres move to increasingly higher densities where the non-interacting gas approximation breaks down. The nuclear interaction is treated at the mean-field level in equations of state

(EoS) commonly used in core-collapse supernova simulations [19, 20]. However, its influence on weak interaction processes is often neglected. In this Letter, we show that a treatment of neutrino-matter interactions that is consistent with the underlying EoS has a strong impact on the spectra and luminosities of the emitted neutrinos. We discuss the relevance for nucleosynthesis, neutrino oscillation studies and neutrino detection.

Our study is based on the work of Ref. [1] where corrections to the opacities due to strong interactions are considered at the mean-field level. Effects of many-body correlations [21] will be considered in a forthcoming publication. They are expected to affect the neutrino spectra at later times [22] than considered in the present study. We focus on charged-current (anti)neutrino absorption processes on neutrons and protons and the inverse reactions:  $e^- + p \rightleftharpoons n + \nu_e$  and  $e^+ + n \rightleftharpoons p + \bar{\nu}_e$ , which are those mainly affected by mean-field corrections.

EoS commonly used in core-collapse supernova simulations, see e.g. Refs. [19, 20], treat neutrons and protons as a gas of quasi-particles that move in a mean-field single-particle potential  $U$ . Assuming non-relativistic nucleons, which is a good approximation for densities  $\rho \leq 5\rho_0$  where  $\rho_0 \approx 2.5 \times 10^{14} \text{ g cm}^{-3}$ , the energy-momentum relation closely resembles the non-interacting case [1]:

$$E_i(\mathbf{p}_i) = \frac{\mathbf{p}_i^2}{2m_i^*} + m_i + U_i, \quad i = n, p, \quad (1)$$

with particle rest-masses  $m_i$ . Both the single-particle mean-field potentials and the (Landau) effective masses,  $m_i^*$  depend on density, temperature and proton-to-nucleon ratio,  $Y_e$ . Importantly, due to the extreme neutron-rich conditions the mean-field potentials for neutron and protons can be very different with their relative difference  $U_n - U_p$  directly related to the nuclear symmetry energy [1].

In order to quantify the impact of the mean field potentials, let us consider (anti)neutrino absorption on neutrons (protons). Assuming zero momentum transfer, i.e.  $\mathbf{p}_n \approx \mathbf{p}_p$  (elastic approximation), the electron(positron) and (anti)neutrino energies are related by:

$$E_{\nu_e} = E_{e^-} - (m_n - m_p) - (U_n - U_p), \quad (2a)$$

$$E_{\bar{\nu}_e} = E_{e^+} + (m_n - m_p) + (U_n - U_p). \quad (2b)$$

Eqs. (2a) and (2b) show that the contribution of the mean field potential reduces (increases) the energy of the emitted neutrinos (antineutrinos). The energy difference between neutrinos and antineutrinos is increased by an amount  $2(U_n - U_p)$ . The opacity, or inverse mean-free path, for (anti)neutrino absorption also changes. In the elastic approximation and assuming extreme relativistic electrons, the opacity for neutrino absorption be-

comes [1, 23]:

$$\chi(E_{\nu_e}) = \frac{G_F^2 V_{ud}^2}{\pi(\hbar c)^4} (g_V^2 + 3g_A^2) \cdot E_e^2 [1 - f_e(E_e)] \frac{n_n - n_p}{1 - e^{\beta(\eta_p - U_p - \eta_n + U_n)}}, \quad (3)$$

with  $E_{\nu_e}$  and  $E_e$  related by equation (2a). The emissivity,  $j(E_{\nu_e})$ , can be obtained from the detailed balance condition  $j(E_{\nu_e}) = \exp(-\beta(E_{\nu_e} - \mu_\nu^{\text{eq}}))\chi(E_{\nu_e})$ , with  $\mu_\nu^{\text{eq}} = \mu_e - (\mu_n - \mu_p)$  the equilibrium neutrino chemical potential,  $\mu$  the chemical potential including rest mass and  $\beta$  the inverse temperature. The opacity and emissivity for antineutrino absorption are obtained exchanging neutron and proton and using equation (2b) to relate the positron and antineutrino energies. In equation (3),  $G_F$  is the Fermi coupling constant,  $V_{ud}$  is the up-down entry of the Cabibbo-Kobayashi-Maskawa matrix,  $g_V$  and  $g_A$  are vector and axial-vector coupling constants and  $n_{p,n}$  the number density of protons or neutrons.  $f$  is the Fermi-Dirac distribution function and  $\eta$  is the chemical potential (without rest mass). The quantity  $\varphi = \eta - U$  represents the chemical potential for a non-interacting gas of nucleons, that is related to the nucleon number density by the relation:

$$n = 2 \int \frac{d^3\mathbf{p}}{(2\pi\hbar c)^3} \frac{1}{e^{\beta(\frac{\mathbf{p}^2}{2m} - \varphi)} + 1}. \quad (4)$$

Eq. (4) provides a method of determining the mean-field potential,  $U$ , when using an EoS that does not provide this quantity, e.g., the EoS of ref. [20].

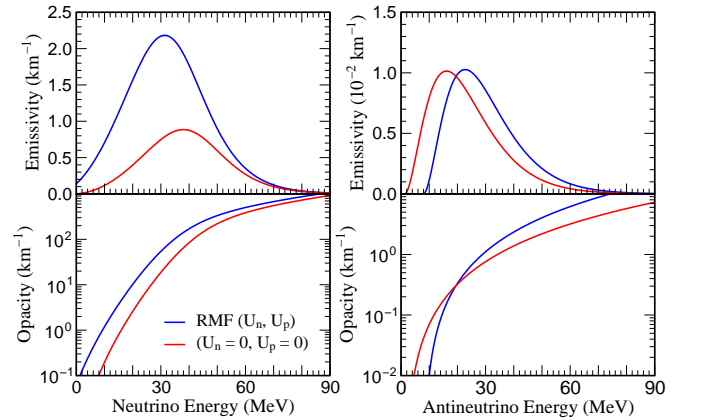


FIG. 1. (Color online) Opacity and emissivity for neutrino (left panels) and antineutrino (right panels), evaluated at conditions  $\rho = 2.1 \times 10^{13} \text{ g cm}^{-3}$ ,  $T = 7.4 \text{ MeV}$  and  $Y_e = 0.035$ .

Figure 1 shows neutrino and antineutrino opacities and emissivities evaluated at conditions found at the antineutrinosphere for the  $18 M_\odot$  model of ref. [12] at 1 s after bounce. The curves labeled RMF ( $U_n, U_p$ ) include the contribution of the mean-field potentials  $U_n = -7.6 \text{ MeV}$  and  $U_p = -14.2 \text{ MeV}$  [20], while the curves labeled

( $U_n = 0, U_p = 0$ ) assume a non-interacting gas of nucleons, i.e. neglect the contribution of the potentials but still use chemical potentials as given by the EoS. Due to the presence of the mean-field potentials the effective  $Q$ -value for electron capture increases with respect to the free case producing neutrinos with substantially lower energy. For the inverse process, neutrino absorption, the opacity is enhanced due to the fact that the produced electron gains an energy  $U_n - U_p$  reducing the final-state Pauli blocking of the electron. The situation is completely analogous to (anti)neutrino emission and absorption on heavy neutron-rich nuclei [24]. Using Eq. (3), it can be shown that the opacity for the non-interacting gas,  $\chi_{\text{ni}}$ , is related to the mean-field opacity,  $\chi_{\text{mf}}$  by  $\chi_{\text{mf}}(E) = \chi_{\text{ni}}(E + U_n - U_p)$ . This relationship produces a large enhancement of the neutrino opacity at high densities,  $\rho \approx 10^{14}$ , where  $U_n - U_p \approx 50$  MeV when compared with the non-interacting approximation used in ref. [12]. For antineutrino absorption, due to the fact that positrons follow Boltzmann statistics, the non-interacting emissivity and mean-field emissivities are related by  $j_{\text{mf}}(E) = j_{\text{ni}}(E - U_n + U_p)$ . The mean-field antineutrino opacity is larger at high densities as final-state Pauli blocking of the neutrons becomes less efficient.

In the following, we explore the impact that a description of opacities consistent with the EoS has on the spectra and luminosities of the emitted neutrinos. We have performed core-collapse supernova simulations based on spherically symmetric radiation hydrodynamics with three-flavor Boltzmann neutrino transport. Since our goal is to explore the differences in neutrino energies and luminosities due to the inclusion of mean-field potentials, we have used a low resolution transport scheme with 12 energy bins and allowed only for radially in and outgoing neutrinos. Despite of its limited resolution, it reproduces the absolute values of luminosities and average energies predicted by higher resolution simulations [16, 17]. Table 1 of [12] list the weak processes considered in our simulations. We use the baryonic high-density EoS from Shen *et al.* [20] for matter in nuclear statistical equilibrium (NSE) at temperatures above 0.45 MeV. As the tabulation of Shen *et al.* does not provide the mean-field potentials, we have computed them using eq. (4). In the non-NSE regime, we use the EoS of ref. [25], which we also use for electrons, positrons and photons in the NSE regime. The simulations are based on the  $15 M_{\odot}$  progenitor of ref. [26]. Because spherically symmetric simulations do not result in explosions for such a massive iron-core progenitor, we enhance the neutrino heating rates in the gain region following the scheme of ref. [17]. It results in the onset of explosion at about 350 ms post bounce. The simulations are evolved from core collapse, through the explosion up to more than 3 seconds after bounce. During core collapse and post-bounce accretion phases, the mean-field potentials,  $U_n, U_p$ , are only on the order of several 100 keV in the region of neutrino decou-

pling, which is located at intermediate densities on the order of  $10^{11} \text{ g cm}^{-3}$ . Hence, the inclusion of mean-field potentials does not affect the supernova dynamics prior to the explosion.

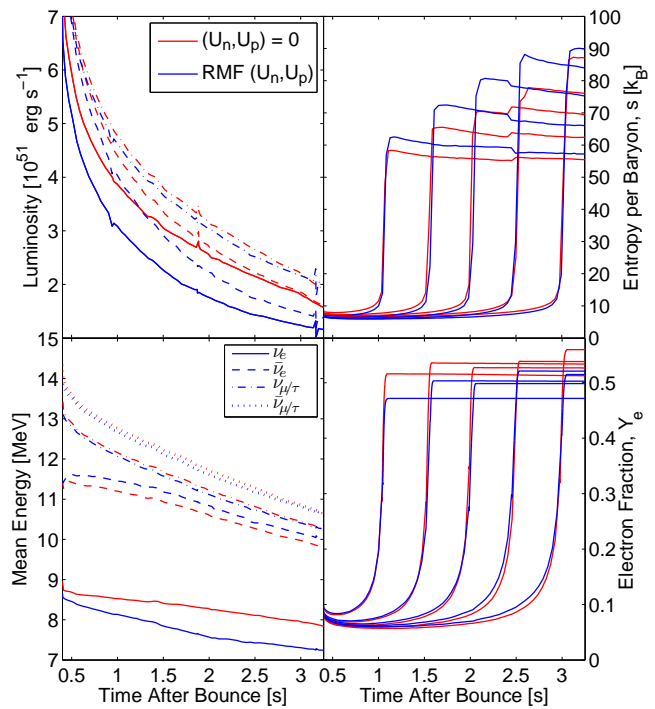


FIG. 2. (Color online) The left panel shows the neutrino luminosity (upper) and average energy (lower) evolution. The right panel shows the evolution of the proton-to-nucleon ratio,  $Y_e$ , and the entropy per nucleon for several mass elements ejected from the PNS surface. The curves shown in blue use neutrino opacities computed using the mean-field potentials of the EoS [20] while they are neglected on the red curves.

After the onset of the explosion the neutrinospheres move to increasingly higher densities reaching values of the order of  $10^{13} \text{ g cm}^{-3}$ . The left panels of Fig. 2 show the evolution of the luminosity and average neutrino energy for all neutrino flavors. These observables are sampled in a co-moving reference frame at a distance of 1000 km. Using charged-current neutrino opacities that include the mean-field potentials slightly reduces the luminosities for all neutrino flavors. Moreover, as expected from the discussion above, it enhances the differences in luminosities and average energies between neutrinos and antineutrinos.

Fig. 3 shows the different neutrino spectra for all flavors at 3 s after bounce at a distance of 30 km outside the neutrinospheres. At this distance neutrinos can be considered free streaming but they have not yet been subject to collective neutrino flavor oscillations [8]. These may result in spectral swaps [27] that occur in regions near to spectral crossings. We expect substantially different oscillation patterns for the spectra obtained with opacities

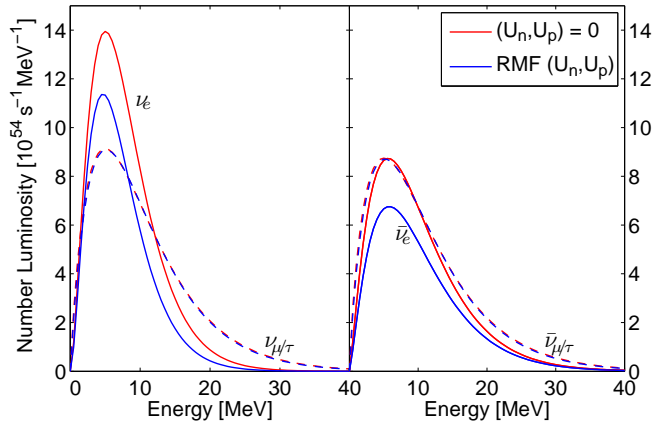


FIG. 3. (Color online) Neutrino spectra for all flavors (solid lines left panel:  $\nu_e$ , dashed lines left panel:  $\nu_{\mu/\tau}$ , solid lines right panel:  $\bar{\nu}_e$ , dashed lines right panel:  $\bar{\nu}_{\mu/\tau}$ ), including the mean-field potentials (blue) and without (red).

consistent with the EoS.

The changes in electron (anti)neutrino spectra and luminosities have important consequences for nucleosynthesis in neutrino-driven winds. The increased difference between average energies of  $\nu_e$  and  $\bar{\nu}_e$  spectra impacts the  $Y_e$  of the ejected matter resulting in slightly neutron-rich conditions for the early ejecta (see lower-right panel of Fig. 2) while at later times the ejecta become proton rich. In the simulation that neglects the contributions of the mean-field potentials the ejecta are always proton-rich. The decrease in  $Y_e$  is not large enough to favor an r-process but may help in the production of isotopes like  $^{92}\text{Mo}$  that are only made under slightly neutron-rich conditions [18, 28]. Also relevant for nucleosynthesis is the slight increase in entropy per nucleon of the ejected material (see upper-right panel Fig. 2) that can be related to the reduced neutrino luminosities [29].

We have shown that a treatment of the charged-current (anti)neutrino opacities, that is consistent with the EoS as suggested by [1], has important consequences for the neutrino-spectra evolution during the PNS cooling phase. The most relevant finding is an increased difference between average energies of  $\nu_e$  and  $\bar{\nu}_e$  that persist during the whole simulation time of 3 seconds after the onset of the explosion. The changes on neutrino spectra are expected to have important consequences for nucleosynthesis, flavor oscillations and neutrino detection on Earth. Our results imply that not only the evolution of the neutrino luminosities [22] but also the spectral differences between  $\nu_e$  and  $\bar{\nu}_e$  are sensitive to the symmetry energy of nuclear matter. Our simulations are based on neutrino opacities computed using the elastic approximation that neglects momentum exchange between nucleons. They need to be extended to consider the full kinematics [1] of the reaction and many-body correlations [21] that are expected to become important at later times than those

considered in the present study. Furthermore, it is important to explore the sensitivity of the results to different EoS and in particular to EoS that are consistent with recent constraints on the nuclear symmetry energy [30].

G.M.P. is partly supported by the Deutsche Forschungsgemeinschaft through contract SFB 634, the Helmholtz International Center for FAIR within the framework of the LOEWE program launched by the state of Hesse and the Helmholtz Association through the Nuclear Astrophysics Virtual Institute (VH-VI-417). T.F. is supported by the Swiss National Science Foundation under project no. PBBSP2-133378. A.L. is supported by the Helmholtz International Center for FAIR and GSI Helmholtzzentrum für Schwerionenforschung. L.H. is supported by the Deutsche Forschungsgemeinschaft through contract SFB 634. We thank fruitful discussions with B. Friman, M. Hempel, H.-Th. Janka, K. Langanke, J. M. Lattimer, M. Liebendörfer, B. Müller, F.-K. Thielemann, and S. Typel.

- 
- [1] S. Reddy, M. Prakash, and J. M. Lattimer, *Phys. Rev. D* **58**, 013009 (1998).
  - [2] H.-T. Janka, *et al.*, *Phys. Repts.* **442**, 38 (2007).
  - [3] K. Hirata, *et al.*, *Phys. Rev. Lett.* **58**, 1490 (1987); M. Koshiba, *Phys. Repts.* **220**, 229 (1992).
  - [4] H. A. Bethe and J. R. Wilson, *Astrophys. J.* **295**, 14 (1985).
  - [5] B. Mueller, H.-T. Janka, and A. Marek, ArXiv e-prints (2012), [arXiv:1202.0815 \[astro-ph.SR\]](#).
  - [6] R. C. Duncan, S. L. Shapiro, and I. Wasserman, *Astrophys. J.* **309**, 141 (1986).
  - [7] Y.-Z. Qian, *Prog. Part. Nucl. Phys.* **50**, 153 (2003).
  - [8] H. Duan, G. M. Fuller, and Y. Qian, *Ann. Rev. Nucl. Part. Sci.* **60**, 569 (2010).
  - [9] S. E. Woosley, *et al.*, *Astrophys. J.* **356**, 272 (1990); A. Heger, *et al.*, *Phys. Lett. B* **606**, 258 (2005).
  - [10] P. Banerjee, W. C. Haxton, and Y.-Z. Qian, *Phys. Rev. Lett.* **106**, 201104 (2011).
  - [11] M. T. Keil, G. G. Raffelt, and H.-T. Janka, *Astrophys. J.* **590**, 971 (2003).
  - [12] T. Fischer, *et al.*, *Phys. Rev. D* **85**, 083003 (2012).
  - [13] S. E. Woosley, *et al.*, *Astrophys. J.* **433**, 229 (1994); K. Takahashi, J. Witt, and H.-T. Janka, *Astron. & Astrophys.* **286**, 857 (1994).
  - [14] R. D. Hoffman, S. E. Woosley, and Y.-Z. Qian, *Astrophys. J.* **482**, 951 (1997).
  - [15] M. Liebendörfer, *et al.*, *Phys. Rev. D* **63**, 103004 (2001); R. Buras, *et al.*, *Astron. & Astrophys.* **447**, 1049 (2006).
  - [16] L. Hudepohl, *et al.*, *Phys. Rev. Lett.* **104**, 251101 (2010).
  - [17] T. Fischer, *et al.*, *Astron. & Astrophys.* **517**, A80 (2010).
  - [18] C. Fröhlich, *et al.*, *Phys. Rev. Lett.* **96**, 142502 (2006); J. Pruet, *et al.*, *Astrophys. J.* **644**, 1028 (2006); S. Wanajo, *Astrophys. J.* **647**, 1323 (2006).
  - [19] J. M. Lattimer and F. D. Swesty, *Nucl. Phys. A* **535**, 331 (1991).
  - [20] H. Shen, H. Toki, K. Oyamatsu, and K. Sumiyoshi, *Nucl. Phys. A* **637**, 435 (1998).
  - [21] S. Reddy, M. Prakash, J. M. Lattimer, and

- J. A. Pons, *Phys. Rev. C* **59**, 2888 (1999); A. Burrows and R. F. Sawyer, *Phys. Rev. C* **58**, 554 (1998); *Phys. Rev. C* **59**, 510 (1999).
- [22] L. F. Roberts, *et al.*, *Phys. Rev. Lett.* **108**, 061103 (2012).
- [23] S. W. Bruenn, *Astrophys. J. Suppl.* **58**, 771 (1985).
- [24] K. Langanke and G. Martínez-Pinedo, *Rev. Mod. Phys.* **75**, 819 (2003).
- [25] F. X. Timmes and D. Arnett, *Astrophys. J. Suppl.* **125**, 277 (1999).
- [26] S. E. Woosley, A. Heger, and T. A. Weaver, *Rev. Mod. Phys.* **74**, 1015 (2002).
- [27] B. Dasgupta, *et al.*, *Phys. Rev. Lett.* **103**, 051105 (2009).
- [28] R. D. Hoffman, *et al.*, *Astrophys. J.* **460**, 478 (1996).
- [29] Y.-Z. Qian and S. E. Woosley, *Astrophys. J.* **471**, 331 (1996).
- [30] J. M. Lattimer and Y. Lim, (2012), [arXiv:1203.4286 \[nucl-th\]](https://arxiv.org/abs/1203.4286).